THE JOURNAL OF PHYSICAL CHEMISTRY C

Article

pubs.acs.org/JPCC

Theoretical Study of the Mechanical Behavior of Individual TiS_2 and MoS_2 Nanotubes

Tommy Lorenz,* David Teich, Jan-Ole Joswig, and Gotthard Seifert

Physikalische Chemie, Technische Universität Dresden, 01062 Dresden, Germany

ABSTRACT: Similar to carbon, several transition-metal chalcogenides are able to form tubular structures. Here, we present results from systematic theoretical investigations of structural and mechanical properties of MoS_2 and TiS_2 nanotubes in comparison to each other, to carbon nanotubes, and to corresponding experimental results. We have obtained the nanotube's Young's moduli (Y), Poisson ratios (ν), and shear moduli (G) as functions of diameter and chirality, using a density-functional-based tight-binding method. Additionally, we have simulated tensile tests by Born−Oppenheimer molecular dynamics simulations. The influence of structural defects on the investigated mechanical properties has been studied as well. As a result of the simulated stretching experiments, we found that TiS_2 nanotubes can be stretched only half as much as MoS_2 nanotubes.

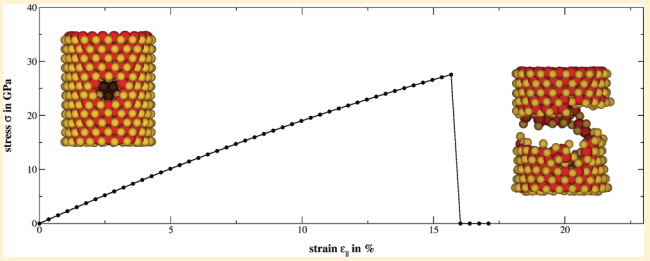

1. INTRODUCTION

Since their discovery in 1991 by Iijima,[1] the interest in carbon nanotubes (CNTs) has been growing continuously. One reason behind this interest may be their exceptional electrical and thermal properties:[2] quasi-one-dimensional, electrical, and thermal conductors constructed from CNTs should have current-carrying capacities that are 1000 times higher than those of copper wires. Another reason are the special mechanical properties of CNTs: by showing Young's moduli of ∼1 TPa,[3] their axial tensile stiffness is much higher than that of every other (nano-) material. During the years following CNT discovery, nanotubes consisting of many other inorganic materials, such as boron nitride, transition metal sulfides, metal oxides, and metal halides,[4,5] have been synthesized. It is assumed by now that nanotubes can be produced from any material that has a layered bulk structure.

Examples for inorganic analogues of CNTs are tubes consisting of tungsten disulfide (WS_2) or molybdenum disulfide (MoS_2). WS_2 nanotubes and fullerene-like nanoparticles, as the first inorganic analogues, were synthesized in 1992.[5] Soon after, corresponding MoS_2 structures were produced as well.[6,7] These two layered bulk materials and their nanotubular structures have been found to be highly related, for the metals are located in the same group in the periodic table. In contrast to carbon nanotubes, WS_2 and MoS_2 nanotubes occur exclusively as multiwall nanotubes and are open-ended. The synthesis is carried out either by arc discharge[8] or by the reduction of the corresponding transition metal oxides (MoO_3, WO_3) with hydrogen sulfide.[9,10] Currently, MoS_2 as a solid-state or nanostructured material is used as a lubricant and catalyst.[11,12]

Likewise, TiS_2 is a layered bulk material. Subsequently, Chen et al. synthesized TiS_2 nanotubes for the first time in 2003.[13,14] Because the bulk material can appear in two different crystal structures with an octahedral or trigonal prismatic coordination of the titanium atoms, nanotubes could be formed out of both structures as well. Similar to MoS_2 and WS_2 nanotubes, TiS_2 nanotubes have several potential applications: they are being investigated as (lithium-intercalated) high-energy storage systems, as cathode material in magnesium-ion batteries,[15] and for catalysis.[14]

In recent years, the electronic and mechanical properties of the inorganic nanotubes mentioned above were investigated in detail experimentally as well as theoretically.[16−24] For example, the absence of small-diameter and single-wall MoS_2 nanotubes could be explained by a phenomenological model based on atomistic quantum-mechanical calculations.[25] In earlier studies, it was reported that all MoS_2 and TiS_2 nanotubes are semiconducting and the electronic properties are diameter- and chirality-dependent.[16,26,29,30] Additionally, chiral MoS_2 and TiS_2 nanotubes show an intrinsic twist[29,30] that slightly stabilizes these structures. Furthermore, first calculations with respect to the influence of structural defects on the properties of such nanotubes have been performed.[31]

In this paper, we report and analyze the structural and mechanical properties of TiS_2 nanotubes. These are compared to the corresponding MoS_2 systems. Additionally, we present new results on the influence of defects on the mechanical properties of MoS_2 nanotubes. Thereby, we will focus on the mechanical behavior of individual single-wall nanotubes. Although experimentally observed nanotubes seem to be exclusively multiwalled, we restrict our study to single-wall nanotubes for two reasons: first, the mechanical and electronic properties of nanotubes are determined to a large extent by the

Received: January 20, 2012
Revised: March 23, 2012
Published: April 26, 2012

   dx.doi.org/10.1021/jp300709w | J. Phys. Chem. C 2012, 116, 11714−11721

strong covalent bonding within the single-wall tubes, because the van der Waals interactions between the walls are only weak; second, from a computational point of view, the system size would increase dramatically for double-wall systems.

In contrast to the MoS_2 system, theoretical studies on TiS_2 are rare, e.g., investigations of structures, strain energies, and electronic properties.[26−29] To our knowledge, there are neither experimental nor theoretical studies of the mechanical properties of this material. Therefore, we have extended the existing studies of TiS_2 nanotubes by investigating their mechanical behavior. At the same time, we have filled the gaps in the studies of MoS_2 nanotubes and performed similar simulations for carbon nanotubes to be able to give a comparative overview of the mechanical properties of both inorganic materials.

A comparison of the results of our simulations with experimental findings is, however, difficult. So far, the Young's moduli of individual WS_2 nanotubes have been measured,[15] and simulations of the corresponding properties of MoS_2 tubes were performed. It was also possible to perform tensile tests of individual multiwall WS_2 nanotubes in experiments.[32,33] Earlier corresponding molecular-dynamics simulations[32,33] and the results presented in this paper are restricted to MoS_2 single-wall nanotubes only. Because tungsten and molybdenum belong to the same group of the periodic table, they show a qualitatively similar mechanical behavior, and experiments as well as simulations of these two materials may be compared. We will follow this route in the present publication as well.

In the following, we will focus first on the three elastic constants (Young's modulus, Poisson ratio, and shear modulus) and, second, on the simulations of stretching experiments to investigate the behavior of tubes under mechanical stress. The influence of structural defects on the elastic constants and on the results of the stretching experiments is briefly discussed for the first time on an atomistic level.

This paper is organized as follows: in section 2 we describe our computational method and derive the calculated elastic constants. In section 3 we discuss structures and energetic properties, the diameter- and chirality-dependence of the elastic constants, the simulation of tensile tests, and the influence of defects. The results are summarized in section 4.

2. COMPUTATIONAL METHODS

For the present study, we have utilized a density-functional tight-binding (DFTB) method,[34,35] for the structural optimization of the investigated nanotubes. It is based on the density functional theory of Hohenberg and Kohn[36] in the formulation of Kohn and Sham.[37] The Kohn−Sham orbitals $\psi_i(\vec{R})$ are expanded in a set of atom-centered basis functions $\varphi_j(\vec{R})$. These functions are determined by self-consistent density functional calculations on the isolated atoms employing a large set of Slater-type basis functions.

The effective one-electron potential in the Kohn−Sham Hamiltonian is approximated as a superposition of the potentials of neutral atoms. Moreover, only one- and two-center integrals are calculated to set up the Hamilton matrix. We have taken a minimal valence basis including the 2s and 2p orbitals for carbon, the 3s and 3p orbitals for sulfur, the 4s, 4p, and 3d orbitals for titanium, and the 5s, 5p, and 4d orbitals for molybdenum. States below these levels were treated within a frozen-core approximation.

To characterize the mechanical properties, three material constants have been considered: the Young's modulus Y, the Poisson ratio ν, and the shear modulus G. The Young's modulus has been calculated from the second derivative of the total energy E with respect to the strain $\varepsilon_{\|}$ at the equilibrium volume V_0:

$$Y = \frac{1}{V_0} \times \frac{\partial^2 E}{\partial \varepsilon_{\|}^2} \tag{1}$$

It indicates how much resistance a sample presents to its deformation under uniaxial strain. Equation 1 additionally contains the volume of the unstressed sample

$$V_0 = 2\pi R_0 L_0 \delta \tag{2}$$

where δ indicates the thickness of the nanotube wall, and R_0 and L_0 are the radius and the length (per unit cell) of the unstrained nanotube. For a carbon nanotube with its monatomic wall, the value of δ is quite ambiguous. Therefore, an area-based Young's modulus Y_S was introduced,[38] in which the volume V_0 is replaced by the cross section $2\pi R_0 L_0$ of the tube:

$$Y_S = \frac{1}{2\pi R_0 L_0} \times \frac{\partial^2 E}{\partial \varepsilon_{\|}^2} = Y\delta \tag{3}$$

However, in order to compare the calculated Young's moduli for carbon nanotubes with experimental values, δ is often chosen as the van der Waals distance in the graphitic lattice (≈3.3 Å[39]). For MoS_2 and TiS_2 nanotubes, the thickness of the triple layer (δ = 6.147 Å) can be used. This value is approximately the distance between the inner and outer cylinders of sulfur atoms, considering the van der Waals radius of sulfur.

As a consequence of the uniaxial elongation or compression, the sample undergoes a deformation perpendicular to the tensile axis (tube axis). The ratio of transverse contraction and axial elongation is described by the Poisson ratio

$$\nu = \frac{\varepsilon_{\perp}}{\varepsilon_{\|}} = -\frac{L_0}{R_0} \times \frac{\partial R}{\partial L} \tag{4}$$

where $\varepsilon_{\|}$ is the externally imposed strain, $\varepsilon_{\perp}$ the lateral contraction, and L_0 and R_0 are defined as above.

The shear modulus is calculated similar to the Young's modulus as

$$G = \frac{\tau}{\gamma} = \frac{1}{V_0} \times \frac{\partial^2 E}{\partial \gamma^2} \text{ with } \gamma = \frac{\varphi R}{L} \tag{5}$$

Here, τ and γ represent the shear stress and the resulting shear angle. If the torsion of the tube is described by a shear of small finite elements on its surface, the shear angle γ can be substituted by an expression containing the torsion angle φ (eq 5). The corresponding G_S values are calculated similarly to Y_S as

$$G = G\delta \tag{6}$$

The Young's modulus and the Poisson ratio were obtained by optimizing the structures at different defined elongations with the conjugate-gradient method. This could be realized by fixing the cell parameter in the axial direction. The largest axial deformations were approximately ±1%. For the calculations of achiral nanotubes, the program package DFTB+[40] with rectangular periodic boundary conditions has been used. Chiral systems and the shear moduli have been calculated using the computer code Trocadero,[41] which is able to consider helical

boundary conditions and can treat chiral structures due to the implementation of objective molecular dynamics.[42−45] Both computer programs contain implementations of the DFTB method.

Tensile tests have been simulated by performing Born−Oppenheimer molecular dynamics (MD) simulations with the DFTB method using the Γ-point approximation within the program package deMon.[46] During the MD simulation, the ends of the tubes were fixed within the periodic simulation box, and a Berendsen[47] thermostat (NVT ensemble, thermostat time constant τ = 0.2 ps) was used to control the temperature. All simulations were performed at T = 300 K. After each equilibration (time step = 2.0 fs, equilibration time =1.5 ps), the resulting structure was stretched by ΔL (in general 0.1 Å). The stretched tube was taken as the initial structure for a following MD simulation with the same set of parameters. This procedure was repeated up to the rupture of the nanotube. The resulting force was calculated as the first derivative of the total energy with respect to the axial cell length. The tensile stress σ was calculated from the ratio of force and cross section.

The elastic constants have been investigated also with respect to the chirality of the tubes. Therefore, we define a tube family as all nanotubes that are described by the integer denominators (n,n), $(n+1,n-1)$, ..., $(2n,0)$. Thus, the (10,10) family consists of the members (10,10), (11,9), (12,8), ..., (20,0), including a zigzag, an armchair, and $n-1$ chiral tubes that all have approximately the same diameter.

3. RESULTS AND DISCUSSION

3.1. Structures. MoS_2 and TiS_2 belong to a class of transition metal disulfides (TMS_2) that form layered bulk materials, in which the individual TMS_2 layers are stacked. Each TMS_2 layer consists of three atomic layers in the order S−TM−S. Within these layers, each transition metal atom is 6-fold coordinated by sulfur atoms. There are two different possibilities to coordinate the TM atoms in this environment: (i) a trigonal prismatic coordination (layer group $p6\bar{m}2$) and (ii) an octahedral coordination (layer group $p3\bar{m}1$), both shown in Figure 1. In their bulk phase, these two structures are labeled 2H and 1T, respectively. Whereas MoS_2 exists as a stable form in the 2H configuration only, TiS_2 crystallizes in both structures, whereby the octahedral coordination is thermodynamically more stable.[26,48] Although the labels 2H and 1T refer to the bulk phase of the material, we will use them to distinguish the monolayered structures in the following.

The lattice constants of the single monolayers were calculated with the DFTB method to validate the parameters. The results are shown in Table 1. The comparison with the experimental values shows a very good agreement. Furthermore, we see from the total energies of TiS_2 that the octahedral coordination is indeed more stable than the prismatic one.

Table 1. Calculated and Experimentally Determined Lattice Constants, Total Energies, And the Strain-Factor β (discussed in section 3.2.) of the Three Investigated Layer Structures

	MoS_2 (2H)	TiS_2 (2H)	TiS_2 (1T)
a (calcd) [Å]	3.273	3.178	3.313
a (exptl) [Å]	3.1602[49]	–	3.407[50]
E_{tot} [eV/atom]	−58.72	−55.62	−55.81
β (calcd) [eV Å^2/atom]	27.2	16.9	11.5

3.2. Strain Energy. Figuratively, the strain energy is a measure of the work to roll up a layer to a tube, i.e., it is the energy difference between the tube and the layer. The strain energy (per atom) as a function of the tube radius R is given by $E_{str} = \beta/R^2$.[51] The individual values of the strain factor β are shown in Table 1. The value for MoS_2 is in good agreement with former calculations.[25] For comparable radii, the strain energies of both TiS_2 structures are significantly lower than for MoS_2 tubes. The strain factors of all TMS_2 nanotubes are much larger than those of carbon nanotubes (for comparison, we have calculated also the strain factor for carbon nanotubes as β_{CNT} = 2.2 eVÅ^2/atom). This fact can partly be explained with structural arguments: The carbon layer is a monatomic layer, whereas the TMS_2 layers have a thickness of three atomic layers (S−TM−S, see inset of Figure 2). Consequently, the (mechanical) work to bend the latter is larger leading to a higher potential energy per atom in the system. Of course, also the strength of the chemical bonds influences the value of β. However, Figure 2 clearly shows that the chirality of the nanotubes does not have any influence on the strain energy.

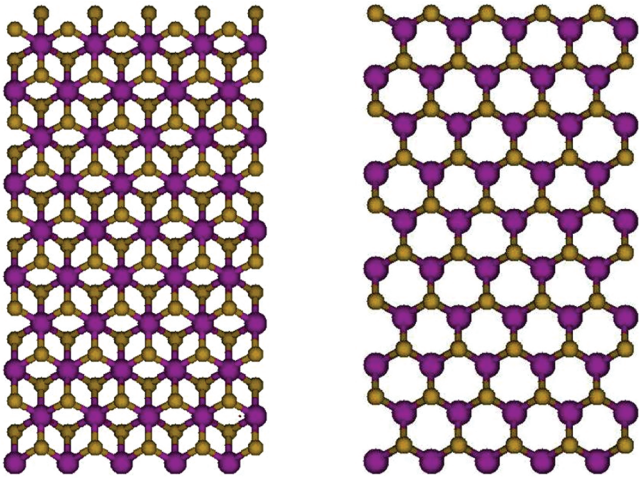

Figure 1. Structures of TiS_2 monolayers of the 1T (left) and 2H (right) TiS_2 bulk phases. The titanium and sulfur atoms are shown as purple and yellow spheres, respectively.

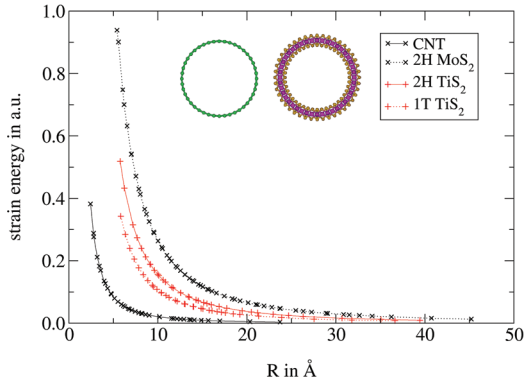

Figure 2. Strain energy as a function of the tube radius R for MoS_2 (dotted black line) and TiS_2 with prismatically (solid red line) and octahedrally (dotted red line) coordinated titanium atoms. For comparison, the calculated strain energies of carbon (solid black line) nanotubes are shown additionally. Inset: (22,0) carbon and TMS_2 nanotubes for visualization of the wall thicknesses.

dx.doi.org/10.1021/jp300709w | J. Phys. Chem. C 2012, 116, 11714−11721

3.3. Elastic Constants. In the following, we discuss our results of the calculations of the elastic constants mentioned in section 2. The elastic constants strongly depend on the tube diameter for thin tubes with diameters lower than 4 nm. With increasing diameter (>4 nm), the elastic constants approach values corresponding to those of the infinite layer structures (cf., Table 2).

Table 2. Calculated Elastic Constants of TMS_2 Nanotubes with the Largest Diameters (8−9 nm), Considered in This Work[a]

	Y (GPa)	Y_S (GPa·nm)	ν	G (GPa)	G_S (GPa·nm)
MoS_2 (2H)	230	141	0.30	88[30]	55
TiS_2 (2H)	272	167	0.16	102	63
TiS_2 (1T)	228	140	0.11	96	59

[a]For the calculation of Y and G, a value of δ = 6.147 Å has been used (see section 2).

Figure 3 shows the surface-based Young's modulus Y_S of different TiS_2 nanotubes as a function of the tube radius R_0.

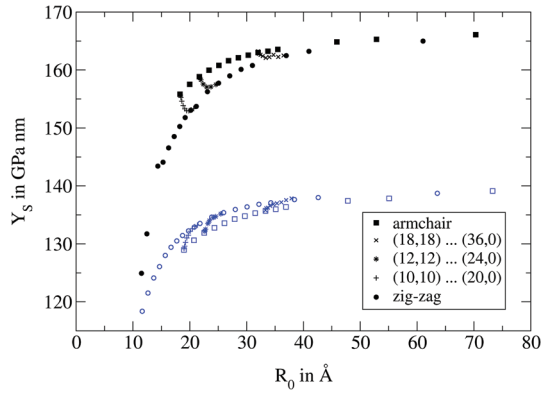

Figure 3. Young's moduli of 1T (blue) and 2H TiS_2 (black) nanotubes as a function of the tube diameter.

The Young's moduli of both TiS_2 structures increase with increasing tube diameter approaching the values of the infinite layers (Table 2). We observe different curve progressions for zigzag and armchair tubes, which are visible especially at small tube diameters. The Young's moduli of the chiral nanotubes lie essentially in between these two limiting curves. For large diameters, the Young's moduli of all chiral and achiral nanotubes approach the same values of the infinite layers.

In comparison to MoS_2 (Figure 4 in ref 30), it turned out that the Y−R curve progression for TiS_2 (Figure 3) slightly differs: the Young's moduli of the MoS_2 zigzag tubes are almost independent of the tube diameter, whereas they are diameter-dependent for the armchair tubes (increasing with increasing diameter; see Figure 4 in ref 30); moreover, the splitting between the Y−R curves of zigzag and armchair nanotubes is larger for MoS_2. The calculated asymptotic limit of the MoS_2 Young's modulus is approximately 230 GPa ($Y_S \approx$ 141 GPa·nm). This value is close to the experimental value for bulk MoS_2 (209 GPa[52]) and to the experimentally received value of monolayered MoS_2.[53] No experimental values are available for TiS_2. We add that we have observed a correlation between the Young's modulus and the band gap in all TMS_2 systems: for comparable diameters, we find a larger Young's modulus for the tube with the larger gap.

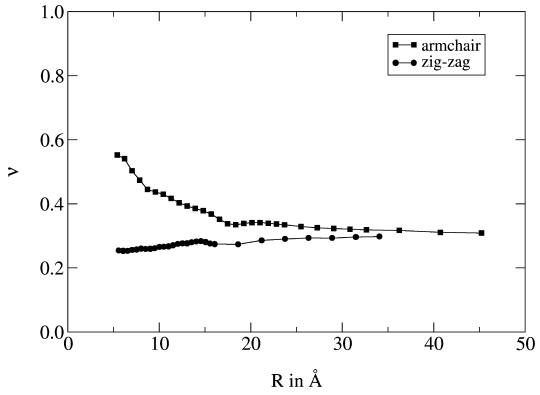

Figure 4. Poisson ratio as a function of diameter for different zigzag and armchair MoS_2 nanotubes.

In earlier studies,[18,30,32,33] the mechanical properties of MoS_2 nanotubes have been investigated. In addition, we present here the calculated Poisson ratios, the stress−strain diagrams, and the influence of defects on these properties. For the Poisson ratios ν and shear moduli G, a similar splitting between zigzag and armchair curves was obtained. As an example, we show in Figure 4 the Poisson ratio as a function of diameter. For MoS_2 nanotubes, the limit of the Poisson ratio for large diameters is about 0.3; this corresponds to the value of the flat layer. As for the Young's moduli,[30] the Poisson ratios of the zigzag MoS_2 nanotubes are nearly independent of the diameter. In contrast, the Poisson ratio of the armchair MoS_2 tubes decreases with increasing diameter, i.e., the transversal contraction decreases with increasing tube diameter.

The shear modulus G describes the resistance of a sample against a shear stress τ. The limits of the calculated shear moduli for all investigated systems are summarized in Table 2. The corresponding G_S for TiS_2 as a function of the radius R are shown in Figure 5 (the corresponding diagram for MoS_2 can be

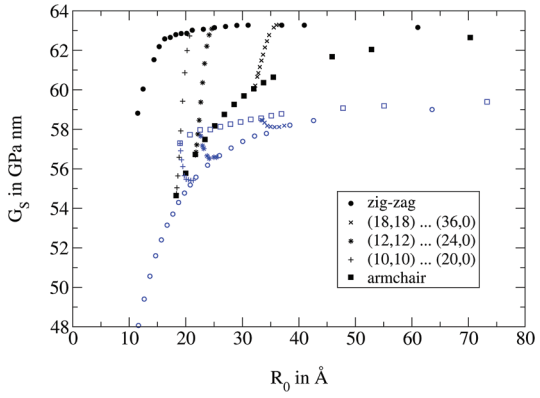

Figure 5. Surface-based shear modulus G_S for 1T (blue, open symbols) and 2H (black, filled symbols) TiS_2 nanotubes.

found in ref 30). The respective location of the armchair and zigzag G_S−R curves is inverted compared to the corresponding Y_S−R curves in Figure 3; that is, if the shear moduli of the armchair tubes are larger than those of the zigzag tubes, it is vice versa for the Young's moduli. We find this for 2H MoS_2 and 1T TiS_2 nanotubes.

3.4. Simulations of Tensile Tests. The Young's modulus describes the linear response of a structure on an external strain giving information only on deformations in the elastic region.

dx.doi.org/10.1021/jp300709w | J. Phys. Chem. C 2012, 116, 11714−11721

However, the nonelastic region up to the rupture of a structure is also of interest. This information can be obtained by tensile tests. In earlier studies,[32,33] tensile tests were performed experimentally on WS_2 nanotubes, and the mechanism of rupture was investigated by MD simulations on defect-free MoS_2 nanotubes. With this contribution, we complement these studies by calculations of stress−strain diagrams for MoS_2 nanotubes in comparison to the results of TiS_2 and carbon nanotubes. Additionally, we have studied the influence of defects. For example, we show in Figure 6 the results of such

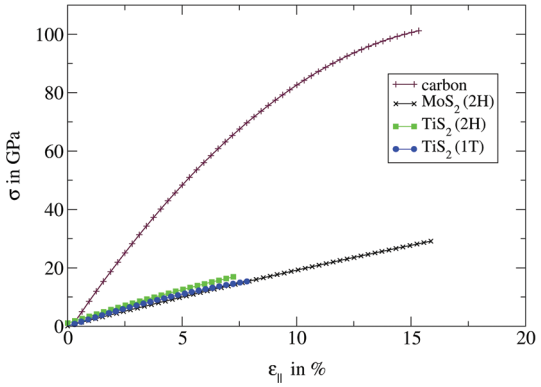

Figure 6. Stress−strain (σ−$\varepsilon_{\parallel}$) diagram for (14,14) TiS_2 and MoS_2 nanotubes obtained from MD simulations as described in section 2. The corresponding stress−strain curve of a (14,14) carbon nanotube is given for comparison. All curves are displayed up to the individual points of rupture.

stress−strain simulations for ideal (14,14) armchair TMS_2 nanotubes. All three systems show slight deviations from linear curve progressions. It can be seen that 2H MoS_2 nanotubes can be stretched up to 16% of their original length before they rupture. In contrast, TiS_2 nanotubes rupture much earlier at elongations of about 6−8% (cf., Table 3).

Table 3. Critical Stress−Strain Parameters of Armchair and Zigzag TMS_2 Nanotubes with Comparable Diameters

				critical values (rupture)	
		Y (GPa)	R_0 (Å)	$\varepsilon_{\parallel}$ (%)	σ (GPa)
MoS_2 (2H)	armchair (14,14)	209.7	13.0	15.9	29.1
	zigzag (22,0)	236.6	12.0	15.4	31.6
TiS_2 (2H)	armchair (14,14)	266.2	12.6	7.2	16.9
	zigzag (22,0)	254.1	11.6	6.1	15.5
TiS_2 (1T)	armchair (14,14)	219.2	13.1	7.8	15.3
	zigzag (22,0)	219.7	11.9	6.1	11.4

For the carbon nanotube, a rather large deviation from the linear stress−strain behavior for small elongations and a much higher tensile stress were obtained compared to those of the TMS_2 nanotubes. The reason for this behavior is the difference in the bonding patterns: Whereas each TMS_2 nanotube consists of an atomic triple layer (S−TM−S), CNTs consist of a single atomic layer only. Therefore, the axial elongation has a direct influence on the C−C bond lengths, whereas the elongation of TMS_2 tubes first and foremost is based on the change of bonding and dihedral angles. This leads, up to a certain level, to smaller stress and a more elastic stress−strain behavior.

Furthermore, the significantly higher Young's moduli of carbon nanotubes explain the higher rupture stress, because a larger Young's modulus leads to a higher force necessary to elongate the nanotube by the same distance. We find this relation also within the same material: the Young's moduli and the rupture stresses of 2H TiS2 nanotubes are higher than those of 1T TiS_2 tubes.

3.5. Influence of Defects. Early experimental investigations of carbon nanotubes have shown that these often have a high defect concentration, which strongly influences their properties.[54−58] Investigations showed that structural defects reduce, for example, the Young's modulus and the tensile stress.[56] In the present work, we have studied the connection between different defects and the mechanical properties of TMS_2 nanotubes. To date, neither theoretical atomistic investigations of the influence of defects on the Young's modulus nor simulations and analyses of tensile tests of defected TMS_2 nanotubes have been published. Exemplarily, we have chosen a set of defects, which are shown and explained in Figure 7.[31]

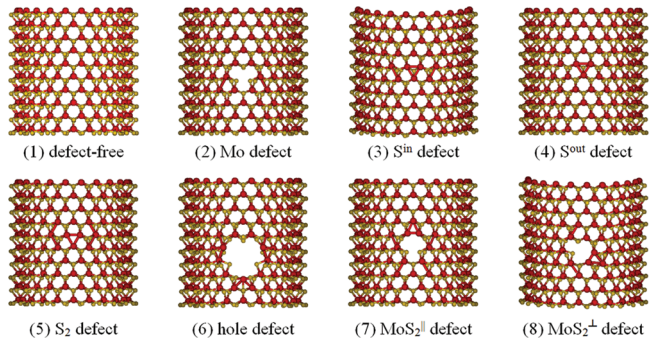

Figure 7. Optimized structures of (22,0) zigzag MoS_2 nanotubes with different structural defects: (1) defect-free, (2) absence of an Mo atom, (3) absence of an S atom from the inner cylinder, (4) absence of an S atom from the outer cylinder, (5) absence of both S atoms, (6) absence of three MoS_2 units, and absence of one MoS_2 unit oriented (7) parallel and (8) perpendicular to the tube axis. In the following, we consider defects 2−5 as small and defects 6−8 as large defects.

All these structures have been fully geometry-optimized for both TMS_2 systems. Depending on the defect, the initial vacancy may be (partly) healed by stronger interactions of the unsaturated edge atoms. This leads, for example, in case of a so-called S_2 defect, to shorter distances of the three neighboring Mo atoms.

However, a significant change of the Young's moduli and Poisson ratios cannot be expected for long nanotubes with a low defect concentration. On the other hand, the selected defects may have a noticeable influence at high defect concentrations. Therefore, we have focused especially on these high concentrations, because the question of whether the influence is large enough to be observed in experiments could not be answered sufficiently yet. The results for a (22,0) MoS_2 nanotube are shown, for example, in Figure 8 and Table 4. At this level of concentration, small defects do not have any significant influence on these properties, because a kind of self-healing leads to an almost intact tubular wall (Figure 7); large defects have a greater influence, because their extent prevents their closure.

To compare the influence of the defects on the different materials, we show in Figure 9 the changes in the Young's

dx.doi.org/10.1021/jp300709w | J. Phys. Chem. C 2012, 116, 11714−11721

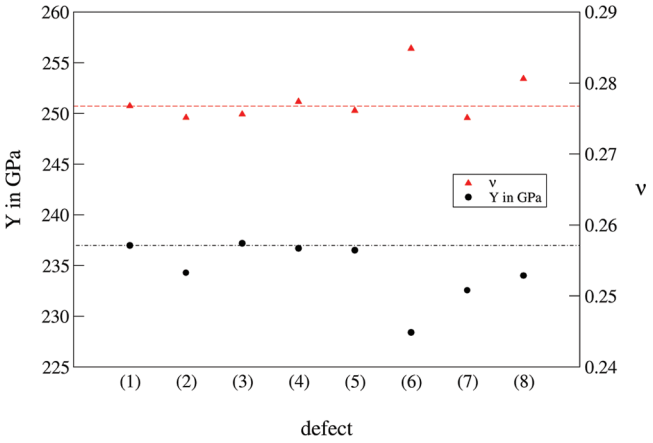

Figure 8. Influence of different structural defects on the Young's modulus (black dots, left ordinate) and the Poisson ratio (red triangles, right ordinate) of a (22,0) MoS_2 nanotube. The values of the defect-free tubes, corresponding to defect 1 are shown as dashed lines. The defects are labeled as in Figure 7. The exact values are given in Table 4.

Table 4. Young's Moduli and Poisson Ratios of a (22,0) MoS_2 Nanotube with and without Defects[a]

defect	Y (GPa)	ΔY (%)	ν	$\Delta\nu$ (%)
(1) no defect	236.78		0.274	
(2) Mo	234.29	−1.05	0.275	0.49
(3) S^{in}	237.20	0.18	0.276	0.67
(4) S^{out}	236.70	−0.03	0.277	1.32
(5) S_2	236.51	−0.11	0.276	0.85
(6) hole	228.40	−3.54	0.285	4.05
(7) $MoS_2^{\parallel}$	232.56	−1.78	0.275	0.48
(8) $MoS_2^{\perp}$	234.01	−1.17	0.281	2.49

[a]The defects are labeled as in Figure 7. The relative deviations are given additionally.

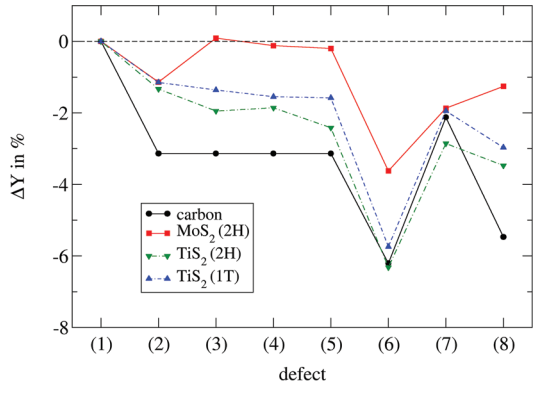

Figure 9. Influence of different structural defects on the Young's modulus of (22,0) nanotubes of the investigated materials. The diagram depicts the relative change of Y with respect to the defect-free tube (ΔY). The defects are labeled as in Figure 7. The lines have been added to guide the eye. Note that the defects 2−5 result in the same structure for carbon nanotubes.

moduli for (22,0) nanotubes with respect to the ideal tubes. TiS_2 nanotubes seem to be more sensitive to small defects than MoS_2 tubes. Furthermore, the Young's moduli of CNTs show the largest responsivity to small defects, which can be explained by structurally hindered self-healing.

The calculated Young's moduli and stress−strain behavior of defect-free MoS_2 nanotubes are in good agreement with the experimentally determined values.[32] For TiS_2, no experimental data is available. Larger deviations in comparison to experimental data[54−58] occur for carbon nanotubes. This raises the following question: do the experimentally synthesized inorganic nanotubes (MoS_2, WS_2) have less structural defects than carbon nanotubes, or is their influence on the mechanical properties simply below the accuracy of the measurement?

To answer this question, tensile tests of MoS_2 nanotubes with the above-described defects were simulated as well. The results are summarized in Table 5. It is apparent that all defects

Table 5. Influence of Structural Defects (see Figure 7) on the Strain of Rupture $\varepsilon_{\parallel}$ and the Rupture Stress σ of a (22,0) Zigzag MoS_2 Nanotube Obtained from the Simulation of Tensile Tests

defect	$\varepsilon_{\parallel}$ (%)	σ (GPa)
(1) no defect	15.67	28.86
(2) Mo	10.68	21.92
(3) S^{in}	11.28	22.18
(4) S^{out}	10.39	17.68
(5) S_2	10.99	21.24
(6) hole	7.09	13.53
(7) $MoS_2^{\parallel}$	10.08	18.74
(8) $MoS_2^{\perp}$	9.50	18.72

have a large influence on both the strain of rupture $\varepsilon_{\parallel}$ and the rupture stress σ. This result indicates that the synthesized TMS_2 nanotubes may indeed have a defect concentration smaller than that of CNTs.

4. CONCLUSIONS

In this paper, we have presented a systematic theoretical investigation of transition metal disulfide nanotubes and their mechanical properties. We have employed a density-functional tight-binding method, which allowed us to study large systems with several hundred atoms. Two different materials have been studied, TiS_2 and MoS_2, where for the latter, two different configurations (2H and 1T) have been considered. Simulations of carbon nanotubes have been performed for comparison.

We found the strain energy of all investigated systems to be chirality-independent. Comparing the systems, it turned out that all TMS_2 nanotubes have larger strain energies than CNTs. MoS_2 nanotubes have the largest strain energy. On the basis of the optimized TMS_2 structures, we have calculated the Young's moduli, the shear moduli, and the Poisson ratios. For small tubes (<4 nm), these strongly depend on the tube diameter. With increasing diameter, these properties approach values corresponding to those of the infinite monolayers. Additionally, the elastic constants are chirality-dependent, and we observe different curve progressions for zigzag and armchair tubes. The elastic constants of the chiral nanotubes lie essentially in between these two limiting curves. For MoS_2, experimental values are available[52] and in good agreement with our results.

Additionally, tensile tests have been simulated up to the rupture of the tubes. We found that MoS_2 nanotubes can be stretched up to 16% and TiS_2 nanotubes up to 6−8% until they break. In comparison, carbon nanotubes show a larger deviation from linear stress−strain behavior and a much higher tensile stress.

dx.doi.org/10.1021/jp300709w | J. Phys. Chem. C 2012, 116, 11714−11721

Finally, we have studied the influence of structural defects on the elastic constants and the stress−strain behavior of the nanotubes. Therefore, we have chosen a set of defects by removing several atoms and calculated the respective properties. The consideration of the selected defects in the nanotubes changes their Young's moduli and Poisson ratios to different extents.

For defect-free MoS_2 nanotubes, we found good agreement between the calculated and the experimentally determined Young's moduli and stress−strain behavior. By simulating tensile tests with MoS_2 nanotubes that exhibit structural defects, we found larger deviations between the calculated and experimental stress−strain behavior. This result indicates that synthesized MoS_2 nanotubes may have a defect concentration smaller than that of CNTs.

AUTHOR INFORMATION

Corresponding Author

*E-mail: tommy.lorenz@chemie.tu-dresden.de.

Notes

The authors declare no competing financial interest.

ACKNOWLEDGMENTS

This work was financially supported by the European Union via ERC grant INTIF 226639. The authors thank Reshef Tenne, Igor Baburin, Knut Vietze, and Andrey Enyashin for fruitful discussions.

REFERENCES

(1) Iijima, S. *Nature* **1991**, *354*, 56−58.
(2) Dresselhaus, M. S.; Dresselhaus, G.; Avouris, Ph. *Top. Appl. Phys.* **2001**, *80*, 287−327.
(3) Treacy, M. M. J.; Ebbesen, T. W.; Gibson, J. M. *Nature* **1996**, *381*, 678−680.
(4) Chopra, N.; Luyken, R.; Cherrey, K.; Crespi, V.; Cohen, M.; Louie, S.; Zettl, A. *Science* **1995**, *269*, 966.
(5) Tenne, R.; Margulis, L.; Genut, M.; Hodes, G. *Nature* **1992**, *360*, 444−446.
(6) Margulis, L.; Salitra, G.; Tenne, R.; Talianker, M. *Nature* **1993**, *365*, 113−114.
(7) Feldman, Y.; Wasserman, E.; Srolovitz, D. J.; Tenne, R. *Science* **1995**, *267*, 222−225.
(8) Chhowalla, M.; Amaratunga, G. A. J. *Nature* **2000**, *407*, 164−167.
(9) Feldman, Y.; Lyakhovitskaya, V.; Tenne, R. *J. Am. Chem. Soc.* **1998**, *120*, 4176.
(10) Remškar, M. *Adv. Mater.* **2004**, *16*, 1497−1504.
(11) Enyashin, A. N.; Gemming, S.; Bar-Sadan, M.; Popovitz-Biro, R.; Hong, S. Y.; Prior, Y.; Tenne, R.; Seifert, G. *Angew. Chem., Int. Ed.* **2007**, *46*, 623.
(12) Gemming, S.; Seifert, G. *Nat. Nanotechnol.* **2007**, *2*, 21−22.
(13) Chen, J.; Li, S.-L.; Tao, Z.-L.; Gao, F. *Chem. Commun.* **2003**, *8*, 980−981.
(14) Chen, J.; Tao, Z.-L.; Li, S.-L. *Angew. Chem., Int. Ed.* **2003**, *42*, 2147−2151.
(15) Tao, Z.-L.; Xu, L.-N.; Gou, X.-L.; Chen, J.; Yuan, H.-T. *Chem. Commun.* **2004**, *18*, 2080−2081.
(16) Tenne, R.; Seifert, G. *Annu. Rev. Mater. Res.* **2009**, *39* (1), 387−413.
(17) Tenne, R.; Remškar, M.; Enyashin, A.; Seifert, G. Inorganic Nanotubes in Fullerene-Like Structures (IF). In *Carbon Nanotubes*; Jorio, A.; Dresselhaus, M. S.; Dresselhaus, G., Eds.; Springer: Heidelberg, 2008.
(18) Kaplan-Ashiri, I.; Cohen, S. R.; Gartsman, K.; Rosentsveig, R.; Seifert, G.; Tenne, R. *J. Mater. Res.* **2004**, *19* (2), 454.
(19) Kalfon-Cohen, E.; Goldbart, O.; Schreiber, R.; Cohen, S. R.; Barlam, D.; Lorenz, T.; Joswig, J.-O.; Seifert, G. *App. Phys. Lett.* **2011**, *98*, 081908.
(20) Kalfon-Cohen, E.; Goldbart, O.; Schreiber, R.; Cohen, S. R.; Barlam, D.; Lorenz, T.; Enyashin, A.; Seifert, G. *J. Vac. Sci. Technol.* **2011**, *B 29* (2), 021009.
(21) Stefanov, M.; Enyashin, A. N.; Heine, T.; Seifert, G. *J. Phys. Chem. C* **2008**, *112* (46), 17764−17767.
(22) Wei, L.; Jun-Fang, C.; Qinyu, H.; Teng, W. *Phys. B* **2010**, *405*, 2498−2502.
(23) Verstraete, M.; Charlier, J.-C. *Phys. Rev. B* **2003**, *68*, 045423.
(24) Kaplan-Ashiri, I.; Tenne, R. *J. Cluster Sci.* **2007**, *18*, 549−563.
(25) Seifert, G.; Köhler, T.; Tenne, R. *J. Phys. Chem. B* **2002**, *106*, 2497−2501.
(26) Ivanovskaya, V. V.; Seifert, G. *Solid State Commun.* **2004**, *130*, 175−180.
(27) Fang, C. M.; de Groot, R. A.; Haas, C. *Phys. Rev. B* **1997**, *56*, 4455.
(28) Enyashin, A. N.; Ivanoskii, A. L. *Inorg. Mater.* **2005**, *41*, 1118−1123.
(29) Teich, D.; Lorenz, T.; Joswig, J.-O.; Seifert, G.; Zhang, D.-B.; Dumitrică, T. *J. Phys. Chem. C* **2011**, *115*, 6392−6396.
(30) Zhang, D.-B.; Dumitrică, T.; Seifert, G. *Phys. Rev. Lett.* **2010**, *104*, 65502.
(31) Enyashin, A. N.; Ivanovskii, A. L. *Semiconductors* **2007**, *41* (1), 81−86.
(32) Kaplan-Ashiri, I.; Cohen, S. R.; Gartsman, K.; Rosentsveig, R.; Ivanovskaya, V.; Heine, T.; Seifert, G.; Wagner, H. D.; Tenne, R. *Mater. Sci. Forum* **2005**, *475−479*, 4097−4102.
(33) Kaplan-Ashiri, I.; Cohen, S. R.; Gartsman, K.; Ivanovskaya, V.; Heine, T.; Seifert, G.; Wiesel, I.; Wagner, H. D.; Tenne, R. *Proc. Natl. Acad. Sci. U.S.A.* **2006**, *103* (3), 523−528.
(34) Seifert, G.; Porezag, D.; Frauenheim, T. *Int. J. Quantum Chem.* **1996**, *58*, 185−192.
(35) Porezag, D.; Frauenheim, T.; Köhler, T.; Seifert, G.; Kaschner, R. *Phys. Rev. B* **1995**, *51*, 12947.
(36) Hohenberg, P.; Kohn, W. *Phys. Rev.* **1964**, *136*, B864.
(37) Kohn, W.; Sham, L. J. *Phys. Rev.* **1965**, *140*, A1133.
(38) Hernández, E.; Goze, C.; Bernier, P.; Rubio, A. *Phys. Rev. Lett.* **1998**, *80* (no. 20), 4502.
(39) Enyashin, A. N.; Gemming, S.; Heine, T.; Seifert, G.; Zhechkov, L. *Phys. Chem. Chem. Phys.* **2006**, *8*, 3320−3325.
(40) DFTBplus, Release *1.1*, http://www.dftb-plus.info.
(41) Rurali, R.; Hernandez, E. *Comput. Mater. Sci.* **2003**, *28*, 85−106.
(42) Dumitrica, T.; James, R. D. *J. Mech. Phys. Solids* **2007**, *55*, 2206−2236.
(43) James, R. D. *J. Mech. Phys. Solids* **2006**, *54*, 2354.
(44) Zhang, D.-B.; Hua, M.; Dumitrica, T. *J. Chem. Phys.* **2008**, *128*, 084104.
(45) Dinga, F.; Harutyunyanb, A. R.; Yakobson, B. I. *PNAS* **2009**, *106* (8), 2506−2509.
(46) Köster, A.; Geudtner, G.; Goursot, A.; Heine, T.; Vela, A.; Salahub, D.; Patchkovskii, S. *deMon*; NRC, Ottawa, Canada, 2004.
(47) Berendsen, H. J. C.; Postma, J. P. M.; van Gunsteren, W. F.; DiNola, A.; Haak, J. R. *J. Chem. Phys.* **1984**, *81*, 3684.
(48) Ivanovskaya, V. V.; Seifert, G.; Ivanovskii, A. L. *Semiconductors* **2005**, *39*, 1058−1065.
(49) Wildervanck, J. C.; Jellinek, F. *Z. Anorg. Allg. Chem.* **1964**, *328*, 309−318.
(50) Thompson, A. H.; Gamble, F. R.; Symon, C. R. *Mater. Res. Bull.* **1975**, *10*, 915−919.
(51) Tibbetts, G. G. *J. Cryst. Growth* **1984**, *66*, 632−638.
(52) Feldman, J. L. *J. Phys. Chem. Solids* **1976**, *37*, 1141−1144.
(53) Bertolazzi, S.; Brivio, J.; Kis, A. *ACS Nano* **2011**, *5*, 9703−9709.
(54) Walters, D. A.; Ericson, L. M.; Casavant, M. J.; Liu, J.; Colbert, D. T.; Smith, K. A.; Smalley, R. E. *Appl. Phys. Lett.* **1999**, *74*, 3803.
(55) Yu, M.-F.; Lourie, O.; Dyer, M. J.; Moloni, K.; Kelly, T. F.; Ruoff, R. S. *Science* **2000**, *287*, 637.

(56) Peng, B.; Locascio, M.; Zapol, P.; Li, S.; Mielke, S. L.; Schatz, G. C.; Espinosa, H. D. *Nat. Nanotechnol.* **2008**, *3*, 626−631.
(57) Yu, M.-F.; Files, B. S.; Arepalli, S.; Ruoff, R. S. *Phys. Rev. Lett.* **2000**, *84*, 5552.
(58) Demczyk, B. G.; Wang, Y. M.; Cumings, J.; Hetman, M.; Han, W.; Zettl, A.; Ritchie, R. O. *Mater. Sci. Eng., A* **2002**, *334*, 173.